Title	Programmable multi-wavelength filter with Mach–Zehnder interferometer embedded in ethanol filled photonic crystal fiber
Author(s)	Zhao, Zhiyong; Tang, Ming; Liao, Huiqi; Ren, Guobin; Fu, Songnian; Yang, Fang; Shum, Perry Ping; Liu, Deming
Citation	Zhao, Z., Tang, M., Liao, H., Ren, G., Fu, S., Yang, F., et al. (2014). Programmable multi-wavelength filter with Mach–Zehnder interferometer embedded in ethanol filled photonic crystal fiber. Optics Letters, 39(7), 2194-2197.
Date	2014
URL	http://hdl.handle.net/10220/19567
Rights	© 2014 Optical Society of America. This paper was published in Optics Letters and is made available as an electronic reprint (preprint) with permission of Optical Society of America. The paper can be found at the following official DOI: http://dx.doi.org/10.1364/OL.39.002194. One print or electronic copy may be made for personal use only. Systematic or multiple reproduction, distribution to multiple locations via electronic or other means, duplication of any material in this paper for a fee or for commercial purposes, or modification of the content of the paper is prohibited and is subject to penalties under law.

Programmable multi-wavelength filter with Mach–Zehnder interferometer embedded in ethanol filled photonic crystal fiber

Zhiyong Zhao,[1,2] Ming Tang,[1,2,*] Huiqi Liao,[1,2] Guobin Ren,[3] Songnian Fu,[1,2] Fang Yang,[1,2] Perry Ping Shum,[4] and Deming Liu[1,2]

[1]*Wuhan National Laboratory for Optoelectronics (WNLO), Huazhong University of Sci&Tech (HUST), Wuhan 430074, China*

[2]*Next Generation Internet Access National Engineering Laboratory (NGIA), School of Optical and Electronic Information, Huazhong University of Sci&Tech (HUST), 1037 Luoyu Road, Wuhan 430074, China*

[3]*Beijing Jiaotong University, Beijing 100044, China*

[4]*Nanyang Technological University, Singapore 637553*

**Corresponding author: tangming@mail.hust.edu.cn*

Received December 26, 2013; revised February 20, 2014; accepted March 6, 2014; posted March 10, 2014 (Doc. ID 203513); published March 31, 2014

We experimentally demonstrated a free spectrum range (FSR) tunable comb filter based on a programmable thermo-controlled Mach–Zehnder interferometer. The device is constructed by sandwiching a length of ethanol-filled photonic crystal fiber between single-mode fibers. A digital thermal printer head is used to facilitate the interference as well as to adjust the phase difference by selectively activating the independent heating elements, thus the FSR can be digitally tuned conveniently. The filter shows a feature of periodic equalized passbands with flat-top steep-edge as well as a high extinction ratio over a very wide range of wavelengths from 1.52 to 1.58 μm.

OCIS codes: (060.5295) Photonic crystal fibers; (130.7408) Wavelength filtering devices; (150.5495) Process monitoring and control; (120.6780) Temperature.

http://dx.doi.org/10.1364/OL.39.002194

Optical comb filters are widely used in wavelength-division-multiplexed optical communication systems, acting as multichannel isolation filters [1] and wavelength selective filters [2], etc. The tunability of such filters is desired to provide flexibility for their practical implementation. In addition, a comb filter with flat-top passbands and a high extinction ratio is indispensable to improve the signal stability, enhance tolerance to wavelength drift, and reduce the adjacent channel crosstalk.

In 1997, Gupta *et al.* [3] reported a computer controlled technique with a thermal head to change fiber Bragg grating's spectral characteristics. In 2004, Li *et al.* [4] demonstrated a tunable filter by heating a chirped grating with a movable resistance wire. A switchable comb filter was then realized by utilizing this method [5]. Petermann *et al.* [6] have reported similar results by replacing the heating wires with a thermal printer head (TPH); however, individual control of each local heating element was not achieved in their work to simultaneously optimize multichannel filtering performance. On the other hand, several approaches based on a Mach–Zehnder interferometer (MZI) have been proposed to implement the flat-top comb filter owning to their simple structure, such as planar lightwave circuit-based parallel-connected unbalanced MZIs [7], double-loop MZIs [8,9], and cascaded all-solid photonic bandgap fiber intermodal MZIs [10]. For the MZI-based comb filters, the tunable range of the free spectrum range (FSR) is very limited and the passbands cannot be configured flexibly to meet various applications.

Recently, we have demonstrated a novel programmable all-fiber structured waveshaper based on linearly chirped fiber Bragg grating and digital thermal controller [11]. The computer controlled TPH adhered with optical fiber is essential to provide digital manipulation. In this work, we propose and experimentally demonstrate a digitally programmable thermo-controlled MZI to achieve a flat-top comb filter with high extinction ratio. The proposed digital optical-comb filter is constructed with a segment of photonic crystal fiber (PCF) filled with ethanol that is sandwiched by single-mode fibers (SMFs). A high density TPH managed by a micro-controller unit (MCU) is used to precisely control the heating position along the ethanol-filled PCF to configure the propagating optical modal profile dynamically. The MZ interference pattern was adjusted by tailoring the interacted mode property and the generated FSR can be digitally tuned conveniently in the wavelength range from 1520 to 1580 nm.

The inset of Fig. 1 shows the cross-sectional view of the PCF (from Yangtze optical fibre and cable company, YOFC, China) used in our experiment, which consists of

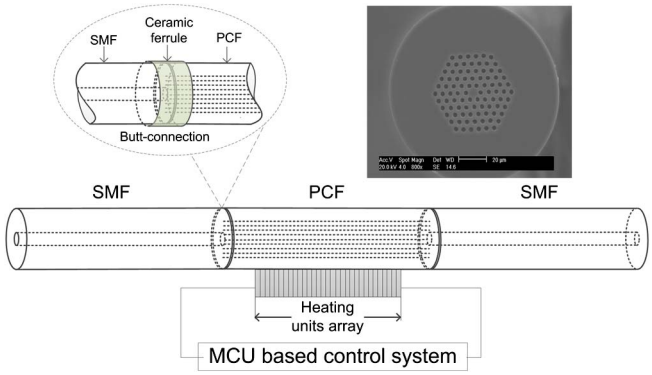

Fig. 1. Schematic diagram of the system configuration. The inset shows the cross sectional view of the PCF.

triangularly arrayed air holes of five layers embedded in pure silica background along the fiber length, as well as a defect with the diameter of 7.2 μm at the fiber center. It has a fiber diameter of 125 μm, air-hole diameter $d = 3.4$ μm and the pitch (center-center spacing) is $\Lambda = 5.8$ μm, so the relative hole-size ratio $d/\Lambda = 0.586$.

The digitized optical-comb filter system is depicted in Fig. 1. An injector is used to infiltrate ethanol into the air-hole region of the PCF and the insertion loss caused by this process is about 3 dB. The coupling between SMF and PCF is accomplished by butt-connection in the ceramic ferrule and bonded by epoxy, thus avoiding large optical loss caused by conventional arc fusion splicing method. The fabricated PCF-based optical filter is then attached to the heating array with a length of 48 mm. The array density is 8 units/mm and each unit is independently controlled by the MCU based system. An amplified spontaneous emission (ASE) light source with a spectrum range from 1510 to 1600 nm was used together with an optical spectrum analyzer (Yokogawa AQ6370C with 0.02 nm best resolution) to measure the spectrum in our experiments. Due to the high thermo-optical coefficient of ethanol (-3.94×10^{-4}/K), which is two orders of magnitude higher than that of pure silica (8.6×10^{-6}/K) at 589.3 nm [12], the effective refractive index of the ethanol-filled PCF can be modulated by thermo-optical effect and a thermo-controlled MZI can be easily achieved with the technique.

When the heating element is in "OFF" state, the measured transmission spectra with and without ethanol is shown in Fig. 2 with black and red curves, respectively. An interference pattern can be observed without ethanol filling and this is widely recognized as the modal interference that has been intensively used for sensing applications [13–15]. The measured refractive index difference between the interacted modes can be obtained from [16]:

$$\Delta\lambda_{\mathrm{FSR}} \approx \lambda^2/(\Delta n_{\mathrm{eff}} \cdot L), \tag{1}$$

where λ is the central wavelength, Δn_{eff} is the effective refractive index difference between the two modes involved in the interference, and L denotes the length of interferometric arm, then Δn_{eff} is calculated to be 8.965×10^{-3}. Simulations based on the finite element method have been performed, as shown in Fig. 3, to point

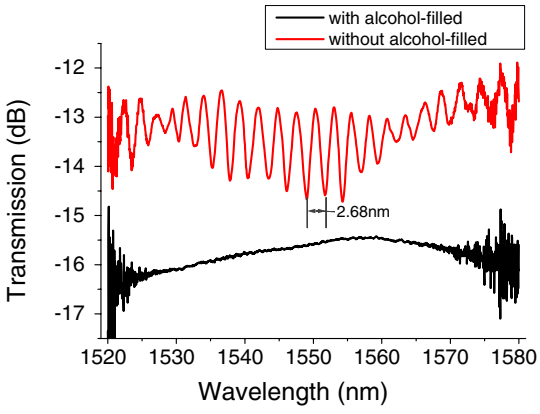

Fig. 2. Transmission spectrum with (black curve) and without (red curve) ethanol filled when no heating was applied.

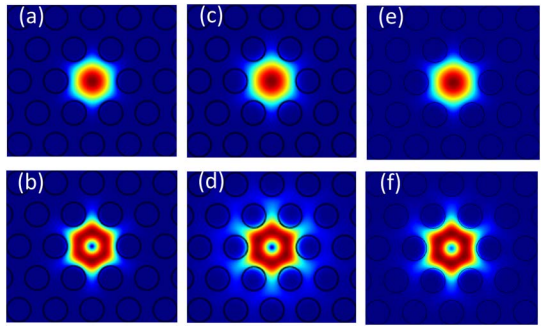

Fig. 3. Transverse mode field intensity distribution, (a), (c), and (e) HE11 mode, (b), (d), and (f) HE21 mode, when w/o ethanol filled (a) and (b), with ethanol filled but w/o heating (c) and (d), and with ethanol filled and heated (e) and (f), respectively.

out that the effective refractive index difference between HE11 mode [Fig. 3(a)] and HE21 mode [Fig. 3(b)] is 9.067×10^{-3}, well matched with the experimental data. It thus confirms that the interference is formed between the HE11 mode and HE21 mode propagating along the PCF. However, with the air cladding filled with ethanol, the reduced core-cladding index difference results in less confinement of HE21 mode. The expanded mode field diameter leads to significantly less coupling efficiency of the HE21 mode at the butt-connection joint. Hence the HE21 mode cannot interfere with HE11 mode effectively in the lead-out SMF, as shown by the black curve in Fig. 2.

When we turn on the thermal control system and locally heat a section of ethanol filled PCF, the refractive index of ethanol will be decreased sharply due to its large negative thermo-optical coefficient at high temperature (~200°C). The enlarged core-cladding refractive index difference helps to squeeze the HE21 mode into the core area. We have deliberately chosen the heating region that is relatively close to the lead-out SMF. Because of the thermal-conductance induced heat diffusion, there is an axial graded index distribution surrounding the heating region, as demonstrated by the thermal image shown in Fig. 4(c). The modified HE11 mode and especially

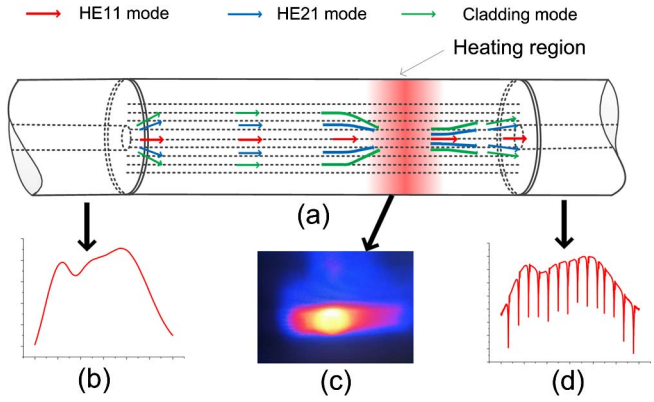

Fig. 4. (a) Schematic diagram of the thermally-induced MZI; (b) and (d) are input spectrum and output spectrum, respectively; (c) is the enlarged view of the heating region from the infrared thermal imaging camera.

HE21 mode can be coupled into the output SMF for interference, as shown in Fig. 4.

Figure 5 shows typical transmission spectra when selectively activating 40, 50, and 60 consecutive heating elements, respectively. The FSR has been adjusted accordingly and the interference patterns demonstrate features of flat-top, steep-edge, and high extinction ratio over a very wide range of wavelength from 1.52 to 1.58 μm. There is also an adjacent transmission notch observed with similar periodicity but less extinction ratio. It is caused by the interference between HE11 mode and another higher-order mode due to the decreased core-cladding index difference of the PCF after filling with ethanol and the mode-field mismatch between SMF and PCF. Actually the superposition of multiple interference patterns contributes to the flattened transmission passband with sharp edge and good extinction ratio, as has been clearly observed in previous reports [7–10].

The resonance condition for the interference can be given by

$$2\pi\Delta nL/\lambda = 2N\pi, \qquad N = 1, 2, 3\ldots \tag{2}$$

The accumulated optical-path difference is determined by the interferometric length, heating length, and temperature change as well as the effective index difference. Then Eq. (2) can be expressed as

$$\Delta n_1\left(\frac{2\pi}{\lambda_2}-\frac{2\pi}{\lambda_1}\right)(L-L') + \int_0^{L'}\Delta n_2(z)\left(\frac{2\pi}{\lambda_2}-\frac{2\pi}{\lambda_1}\right)\mathrm{d}z = 2\pi, \tag{3}$$

where λ_1 and λ_2 are the wavelengths of two adjacent resonance peaks, L denotes the length of interferometric arm and L' is the heating length (heat diffusion length is included), Δn_1 is the modes refractive index difference without heating, $\Delta n_2(z)$ is temperature-dependent index difference along the heating region so it is a (z)-dependent variable along fiber axial position. Equation (3) can be simplified as

$$\Delta n_1(L-L') + \int_0^{L'}\Delta n_2(z)\mathrm{d}z \approx \frac{\lambda^2}{\Delta\lambda_{\mathrm{FSR}}}. \tag{4}$$

It is realized from Eq. (4) that the FSR will decrease by increasing either heating temperature or heating length. Since $\Delta n_2(z)$ is larger than Δn_1, we can get the inequality from Eq. (4) as $\Delta n_1 L \le \lambda^2/\Delta\lambda_{\mathrm{FSR}}$. Δn_1 can thus be calculated as 6.854×10^{-3}, 8.011×10^{-3}, and 8.616×10^{-3} from the experimental data of Fig. 5, respectively. Theoretically, the measured refractive index difference should fall in the simulated values between 7.294×10^{-3} (without heating) and 8.082×10^{-3} (with entire PCF heated). The reasonable error may be caused by the thermal expansion of the ethanol material.

In addition, the heating strength is controlled by the duty ratio of the driving electrical pulse sent from MCU. The temperature can be adjusted with this pulse-width modulation. Since both the MCU system and the ethanol infiltrating technique are mature, the whole device is reproducible for repeatable experiments. The same heating parameters produced identical spectrum and the maximal FSR deviation was measured to be less than 0.05 nm at steady state, which indicated its good repeatability. One of the key advantages of our proposed comb filter is that the optical phase difference can be conveniently programmed using the digital thermal controller. Therefore an FSR tunable comb filter has been achieved by configuring heating parameters. The flat-top passband presented in our experiment is very useful in today's large capacity, dense wavelength division multiplexed optical-communication system because the spectrum width of each channel becomes wider by using a higher-order modulation format. It may also find potential applications in tunable multichannel notch filters. The detailed characteristics of filters presented in Fig. 5 are shown in Fig. 6, where the horizontal axis

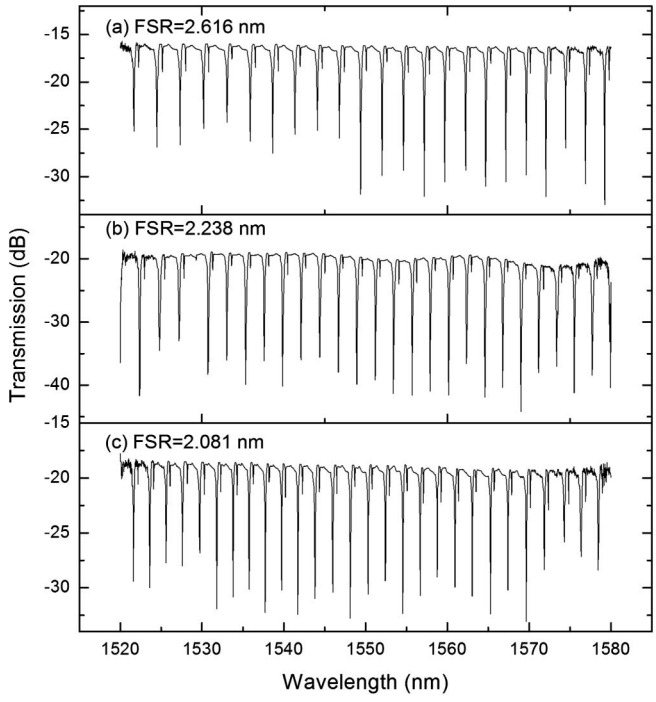

Fig. 5. Transmission spectra with different heating lengths (a) 5 mm, (b) 6.25 mm, (c) 7.5 mm, and the FSRs are 2.616 nm, 2.238 nm, and 2.081 nm, respectively.

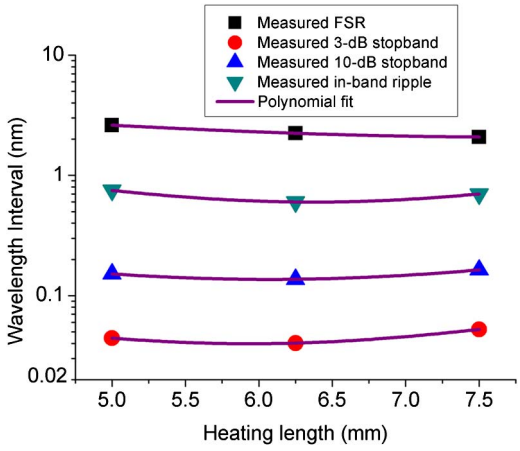

Fig. 6. Properties of the filters, the y axis is shown on a logarithmic scale.

represents the physical heating length, and heat diffusion length is not included.

In conclusion, we proposed and demonstrated a programmable digital optical fiber comb filter with flat passband and high extinction ratio. The digital comb filter is constructed by ethanol-filled PCF and precise thermal controller. The thermo-optical effect of ethanol-filled cladding region and the tailored mode profile are essential to achieve such a FSR tunable reconfigurable optical fiber filter.

This work is supported by the National Natural Science Foundation of China (Grant Nos. 61107087 and 61331010), the 863 High Technology Plan of China (2013AA013402), the National Basic Research Program of China (973 Program: 2010CB328305) and the Fundamental Research Funds for the Central Universities', HUST: 2013TS052. The authors would like to extend their thanks to Dr. Weijun Tong and Dr. Huifeng Wei from YOFC Company, China, for providing the PCF and fruitful discussions.

References

1. X. J. Gu, Opt. Lett. **23**, 509 (1998).
2. A. Luo, Z. Luo, and W. Xu, Opt. Lett. **34**, 2135 (2009).
3. S. Gupta, T. Mizunami, and T. Shimomura, J. Lightwave Technol. **15**, 1925 (1997).
4. S. Y. Li, N. Q. Ngo, S. C. Tjin, P. Shum, and J. Zhang, Opt. Lett. **29**, 29 (2004).
5. N. Q. Ngo, D. Liu, S. C. Tjin, X. Dong, and P. Shum, Opt. Lett. **30**, 2994 (2005).
6. I. Petermann, S. Helmfrid, O. Gunnarsson, and L. Kjellberg, J. Opt. A **9**, 1057 (2007).
7. Q. Wu, P. L. Chu, H. P. Chan, and B. P. Pal, IEEE Photon. Technol. Lett. **17**, 2619 (2005).
8. A. Luo, Z. Luo, W. Xu, and H. Cui, Opt. Express **18**, 6056 (2010).
9. H. Meng, X. Wu, W. Shen, and X. Huang, IEEE Photon. Technol. Lett. **24**, 206 (2012).
10. Y. Geng, X. Li, X. Tan, Y. Deng, and Y. Yu, Opt. Express **21**, 17352 (2013).
11. H. Zhang, M. Tang, Y. Xie, H. Liao, S. Fu, P. P. Shum, and D. Liu, Appl. Phys. B **112**, 479 (2013).
12. Y. Yu, X. Li, X. Hong, Y. Deng, K. Song, Y. Geng, H. Wei, and W. Tong, Opt. Express **18**, 15383 (2010).
13. S. H. Aref, R. Amezcua-Correa, J. P. Carvalho, O. Frazão, P. Caldas, J. L. Santos, F. M. Araújo, H. Latifi, F. Farahi, and L. A. Ferreira, Opt. Express **17**, 18669 (2009).
14. S. M. Nalawade and H. V. Thakur, IEEE Photon. Technol. Lett. **23**, 1600 (2011).
15. Z. Wu, Y. Liu, Z. Wang, T. Han, S. Li, M. Jiang, P. Ping Shum, and X. Quyen Dinh, Appl. Phys. Lett. **101**, 141106 (2012).
16. L. V. Nguyen, D. Hwang, S. Moon, D. S. Moon, and Y. Chung, Opt. Express **16**, 11369 (2008).